Analysis of Severly Damaged RCC Column through Cast-In-Situ Vs Prefabricated Solution

Nagendhiraprabhu. K[1], J.Ranjith Singh[2] gokulram.H[3] And Geethakumari.D[4]

[1]PG student, Department of Civil Engineering ,CSI COLLEGE OF ENGINEERING , KETTI ,Tamilnadu, India
[2,3,4]Assistant professor , Department of Civil Engineering, CSI COLLEGE OF ENGINEERING , KETTI,Tamilnadu, India

ABSTRACT
In present the results of an analytical aimed to develop and study the axial load bearing performance of damaged columns using cast-in-situ (HCP) Hybrid Composite Panels. The effectiveness of prefabricated hybrid Composite plates (HCPs) as a seismic retrofitting solution for damaged interior RC beam- column joints is analytically studied. HCP is composed of a thin plate made of strain hardening cementation composite (SHCC) reinforced with CFRP sheets/laminates. Two full-scale severely damaged interior beam-column joints are retrofitted using two different configuration of HCPs. The effectiveness of these retrofitting solutions mainly in terms of hysteretic response, dissipated energy. According to these criteria, both solutions resulted in superior responses regarding the Ones registered in their virgin states. To study the axial load bearing performance of reinforced column under various deficiencies – 20%,40%, 60%... parameters taken for study are different deficiencies of the columns, number of layers and number of bolts and their pattern output research like ultimate axial load, ultimate deflection, load vs deflection comparison, Percentage of strength are studied.
Keywords: Column damage ,HCP,Column joint ,Repair ,Interaction ,Confinement ,CFRP

I.   INTRODUCTION

Composites are now common materials in retrofitting existing under-designed RC structures. The use of Fiber Reinforced systems has been on the focus of many studies since the early 70s even though a broad use of the technique started much later. Until lately, composite materials used for rehabilitation of concrete or masonry structures were generally applied through organic matrix (epoxy-based), guaranteeing a significant improvement for both resistance and ductility properties of the strengthened element.

Confinement is one of the main techniques used to retrofit axially loaded elements. Fiber Reinforced polymer (FRP) systems permit to easily confine existing RC elements by wrapping continuously or partially FRP strips, enhancing their axial strength and ductility without a significant increase in weight or lateral stiffness. Confinement by FRP systems has proven to be effective also for repairing RC elements damaged due to excessive axial loading or seismic events. Several research works have been carried out to investigate repair effectiveness of FRP confinement both on plain and reinforced concrete. Saadatmanesh et al investigated the effectiveness of repairing earthquake-damaged RC columns with FRP wraps. Four different specimens were tested under lateral cyclic loading to simulate the seismic effect on the elements, which were then repaired through FRP wraps and retested under the same protocol. In general, all repaired specimens performed well under the cyclic loading test, showing an increase in lateral strength varying from 1 to 38%. Li et al. conducted an experimental campaign on 24 RC specimens tested under uniaxial compression that were formerly damaged through split tensile tests. On the other hand, Faleschini et al. investigated experimentally the effectiveness of FRP composites to repair severely damaged exterior RC beam-column joints, verifying also the contribution of the FRP system on the overall shear capacity of the joints through some analytical models. Some researchers have also experimentally investigated the effect of the combined FRP-steel confinement on the behavior

of concrete columns. Eid & Paultre presented a designed-oriented confinement model for assessing the axial and lateral behavior of circular concrete columns confined with steel ties, FRP composites, and both of them. Teng et al proposed a stress–strain model for concrete under combined confinement from FRP and TSR, which has been derived in two alternative versions seeking for increasing accuracy of the prediction. Subsequently, Lin et al presented a design-oriented stress–strain model for concrete under the combined FRP-steel confinement for circular RC columns, showing a good balance between accuracy of the prevision and simplicity of form. AlRahmani & Rasheed proposed a confinement model for combined external FRP – internal TSR confinement for rectangular RC columns. Lately, Kaeseberg et al conducted an extensive experimental research on 63 CFRP-confined plain concrete columns and 60 CFRP-TSR confined specimens, analyzing the influence on the confinement efficiency of different parameters. Finally, a modified stress–strain and ultimate condition design model was proposed.

However, the use of epoxy resins brings some important liabilities to FRP systems. Poor fire resistance difficult application on wet surfaces, low breathability of the substrate, low reversibility and high sensitivity to UV radiations have led to a lower use of FRP systems in favor to new, more compatible and durable solutions. A similar but alternative solution was born from replacing the organic (epoxy) matrix with inorganic cement-based one, generally known as Fiber Reinforced Cementitious Mortar (FRCM) or Textile Reinforced Mortars (TRM). Like FRP systems, FRCMs have been broadly used lately to enhance flexural and shear strength of beam elements and to enhance axial strength and ductility of concrete or masonry columns through confinement.

Concrete confinement through FRCM systems has been the subject of many experimental campaigns and research activities. Tests are mainly based on small-scale non-reinforced elements. Triantafillou et al. were one of the first to analyze the effectiveness of confinement through TRM with respect to the more consolidated FRP systems. Results proved that TRM jackets provided a significant increase in strength and ductility to plain concrete specimens, even though this solution resulted slightly less effective than the FRP counterpart. More recently, Colajanni et al. analyzed the effect of fiber ratio, cross-section shape and corner radius in FRCM confined specimens tested under monotonic and cyclic axial loading. Ombres et al. conducted several

experimental campaignson small-scale plain concrete specimens confined with FRCM systems and later proposed a prediction model based on experimental data collected from different research works. Gonzalez-Libreros et al. also analyzed confinement of plain concrete specimens using CFRCM and GFRCM (the former with carbon, and the latter with glass fibers). The investigation included also the monitoring of hoop strains developed on fibers, to better understand the influence of fiber properties on the FRCM confinement effectiveness. The study showed that fiber exploitation ratio and final confinement effectiveness strongly depends on fabric properties used in the FRCM system. On the other hand, less experimental work can be found on FRCM confinement of real-scale reinforced concrete elements. Bournas et alinvestigated confinement effectiveness of FRCM on small-scale RC specimens tested under uniaxial compression loading and on nearly full-scale RC columns tested under cyclic lateral loading. Results showed that FRCM jacketing effectiveness was similar to that of specimens confined with FRPs even though a slight difference of nearly 10% was observed on the uniaxial compressive tests. Recently, some of the authors have investigated confinement effectiveness of FRCM systems on full-scale RC columns comparing different cross-section shapes and steel reinforcement configurations using carbon fibers and glass fibers. Both studies investigated strain development both on transverse steel reinforcement and on confining fibers to evaluate the influence of the axial rigidity of the composites on the effectiveness of the FRCM system and the interaction between internal transverse steel reinforcement and the external FRCM confinement.

While FRCM systems have proven to confer an adequate level of confinement to existing concrete elements, little work has been done to evaluate their effectiveness in the repair of damaged RC elements by excessive axial loads or, as often happens, by seismic loads. Few studies have been carried out on small-scale plain concrete specimens, worth mentioning Peled who studied confinement of damaged and undamaged concrete elements with FRP and FRCM systems. Results showed that composite systems were able to provide an adequate enhancement of axial strength and ductility even for specimens with initial damage conditions. The effectiveness was observed also by Gonzalez-Libreros et al. where small-scale plain concrete specimens were initially damaged through post-peak compressive loading, then confined by CFRCM and re-tested under

monotonic axial load. Results showed that CFRCM confinement was able to restore the original axial capacity of the specimens.

However, on the best authors' knowledge, the few experimental works cited above on the effectiveness of FRCM jackets on damaged axially-loaded columns dealt only with small scale specimens, and considered only plain concrete (without any internal reinforcement). The present paper's goal is to investigate the effectiveness of CFRCM composites to adequately repair severely damaged RC columns. The experimental campaign considers different cross-section shapes (circular and squared), different internal reinforcement configurations and compares the results of unconfined RC members, CFRM confined specimens with undamaged conditions (strengthened) and CFRCM confined specimens with severe damage conditions (severely-damaged and repaired). In addition, hoop strains of transverse steel reinforcement (TSR) and external fiber reinforcement have been investigated to better understand fiber exploitation and steel-fiber interaction in specimens with different initial conditions.

II. MATERIALS AND EXPERIMENTAL PROGRAM

2.1. Test specimens

The research program deals with the study of nine RC samples, which differ by the following variables: cross-section shape; inner transverse reinforcement amount; concrete damage presence or not; presence of FRCM jacket or not. Specimens' main features are described in Table 1. Overall, it is possible to classify them in three main categories: unconfined; strengthened; severely damaged and repaired.

All the columns present the same height h = 1000 mm and concrete cover c = 20 mm. Two cross-section geometries are investigated, a circular one C with diameter d = 300 mm; and a squared one S with size l = 300 mm. In this latter case, the same corner radius r of 20 mm was used in all the prismatic columns. Concerning the inner reinforcement, details are shown in Fig. 1: there, it is possible to observe how for all the test specimens the same longitudinal steel reinforcement (A_{sl}) is adopted, consisting in four 14mm diameter bars, equally spaced in the cylinders and placed at section edges in the prisms. Conversely, the amount of TSR (A_{sw}) varies adopting two configurations. Cylinders present only one single TSR type, consisting in circular hoops with 8-mm diameter bars, placed each 200 mm in the central part of the specimen. Two legged stirrups with 8-mm diameter bars are used instead

Table 1
Specimens characteristics.

| Specimen ID	Geometry				Steel Reinforcement B450C		Concrete		FRCM Confinement		
	Section geometry Concrete	Specimen dimensions Presence Number of		Corner radius	A_{sl}		A_{sw} (mm²/	Concrete		batch	f_{cm}
		(mm)			(mm²)	m)	(MPa)	Damage		layers	
C20_NC	circular	d = 300; h = 1000	–		615	502	17.4	–	no	–	
S20_NC	Square	l = 300; h = 1000	20		615	502	17.4	–	no	–	
S33_NC	Square	l = 300; h = 1000	20		615	301	24.1	–	no	–	
C20_D0_C2	circular	d = 300; h = 1000	–		615	502	17.4	–	yes	2	
S20_D0_C2	Square	l = 300; h = 1000	20		615	502	17.4	–	yes	2	
S33_D0_C2	Square	l = 300; h = 1000	20		615	301	24.1	–	yes	2	
C20_D1_C2	circular	d = 300; h = 1000	–		615	502	17.4	yes, 70%	yes	2	
S20_D1_C2	Square	l = 300; h = 1000	20		615	502	17.4	yes, 70%	yes	2	
S33_D1_C2	Square	l = 300; h = 1000	20		615	301	24.1	yes, 70%	yes	2	
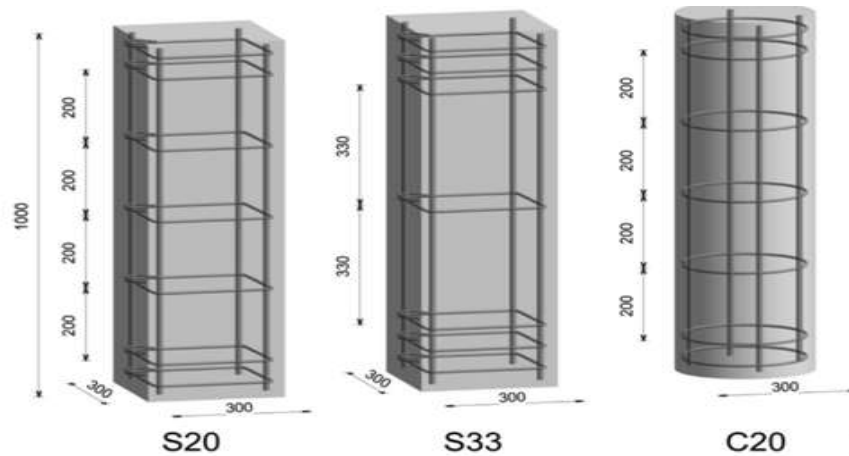
Fig. 1. Reinforcement details.

in prismatic specimens, adopting two spacings in central region of the columns, namely 200 and 330 mm. Steel reinforcement bar properties were the same for all the configurations, and they were experimentally evaluated on three specimens per each type through tensile tests, being $f_y = 552 \pm 10$ MPa at $e_y = 0.002$, $f_t = 6\ 50 \pm 15$ MPa at $e_t = 0.090$ for the longitudinal 14-mm diameter bars, and $f_y = 485 \pm 15$ MPa at $e_y = 0.002$, $f_t = 630 \pm 18$ MPa at $e_t = 0.090$ for the transverse 8-mm diameter bars, respectively.

To realize the specimens, two different concrete batches were used due to laboratory constraints, aiming in both cases at attaining a cylinder compressive strength class at 28 days of about C16/20 according to that however present some differences in terms of strength and elastic properties in the two mixes. Indeed, the following experimental results (evaluated on three specimens per type and per each analyzed feature, i.e., compressive strength, tensile strength and secant elastic modulus, at 28 days) were obtained: $f_{c1} = 24.1 \pm 0.74$ MPa, $f_{ct1} = 1.15 \pm 0.26$ MPa, $E_{c1} = 33.3 \pm 4.25$ GPa for the first batch; $f_{c2} = 17.4 \pm 2.04$ MPa, $f_{ct2} = 1.10 \pm 0.14$ MPa, $E_{c2} = 19.2 \pm 0.95$ GPa for the second one. It is worth to recall that each trio of unconfined, confined and damaged-repaired specimens is realized with the same mix, for sake of comparison purposes. Further, three columns are labelled as damaged ones, this meaning that damaged specimens are the same unconfined columns (named as NC) subject to the loading protocol (described in Section 2.3) and then repaired. Hence, a direct comparison between the performance of unconfined and damaged-repaired specimens is possible.

Lastly, the specimens could be unconfined or confined, and in this latter case the FRCM jacket is realized through two-fiber layers of carbon-

FRCM composite, which characteristics are reported in Section 2.2. The two-layers confinement choice was made based on a previous experimental campaign carried out by some of the authors on damaged plain concrete cylinders confined with the same fiber type obtaining strength enhancement between 10 and 20% when using this confinement configuration Overall, six samples over nine were confined.

2.2. Externally-bonded composite properties

The FRCM system was realized using balanced bidirectional carbon fiber sheets and a single-component mortar (CFRCM system). The fibers' characteristics declared by the producer were integrated by some experimental tests, needed to experimentally assess the tensile strength (f_u) and elastic modulus (E_f) values. To sum up, the properties of the carbon fiber, resulted from tests on three specimens, are: overall area weight $W = 170$ g/m^2, fiber elastic modulus $E_f = 242$ GPa, fiber tensile strength $f_u = 1487$ (MPa) at ultimate tensile strain $e_{fu} = 1.1\%$, equivalent nominal thickness $t_f = 0.047$ mm. The mortar is a fiber-reinforced pre-mixed one, hydrated at a water/binder ratio ranging between 0.18 and 0.22. For the repair operation, the same mortar was used. Mechanical properties (compressive and flexural strength) were experimentally evaluated according to EN 1015–11 on 40x40x160 mm prisms that were casted during the repair and strengthening operations, and tested the same day of RC columns, and they are reported in Table 2 per each realized column. Values refer to average results measured at least on three samples per each analyzed property.

2.3. Experimental protocol: loading, test setup, repair and retrofit operations

The same experimental loading protocol was used for all the tested specimens, and it involves an axial loading of the columns through a displacement-control mode, during which concrete axial strains ($e_{c,yy}$), strains into both TSR ($e_{s,xx}$) and CFRCM fibers ($e_{f,xx}$) were simultaneously acquired. The load was applied at a rate of 0.3 mm/min, similarly than in directly onto the top of the RC column, using a a 10MN capacity testing machine which mounted a 6MN capacity load cell

for the continuous acquisition of the signal. In the unconfined specimens, the load was stopped after a pre-imposed damage condition of about 30%, identified as the point in the post-peak branch corresponding to the 0.70 of the peak load (P_{max}), was reached. Such damage level is considered very significant, also compared to other works in literature aimed at verifying the effectiveness of repair systems to damaged RC specimens, where typically such value is set around 20% but might arise up to 50% .

Table 2
FRCM and repair mortar properties.

	q (kg/m^3)	f_{cm} (MPa)	$f_{cm,f}$ (MPa)	q (kg/m^3)	f_{cm} (MPa)	$f_{cm,f}$ (MPa)
C20_D0_C2	1880 ± 22	30.88 ± 0.78	5.08 ± 0.27	–	–	–
S20_D0_C2	1877 ± 12	32.14 ± 0.62	6.12 ± 0.94	–	–	–
S33_D0_C2	1947 ± 11	33.56 ± 1.81	5.50 ± 1.06	–	–	–
C20_D1_C2	2046 ± 34	21.06 ± 1.39	4.96 ± 0.26	2153 ± 5	22.81 ± 3.76	5.93 ± 0.27
S20_D1_C2	2114 ± 48	23.22 ± 1.62	4.77 ± 0.37	2143 ± 40	21.58 ± 1.59	5.08 ± 0.36
S33_D1_C2	2047 ± 19	20.71 ± 1.16	4.92 ± 0.43	2091 ± 78	28.20 ± 2.30	5.41 ± 0.90

Concerning the instrumentation used to acquire concrete axial strains, they were monitored using two types of devices, mechanical strain gages (mSGs) to describe the pre-peak and linear voltage displacement transducers (LVDTs) to better capture the post-peak branch. Three mSGs, with a gauge length of 250 mm, were mounted onto the columns (cylinder) external surface at midheight, equally spaced at 120. In case of prismatic samples, four mSGs were used, with the same characteristics, but placed onto each sample face. Further, two LVDTs were adopted to measure the movement of the plate mounted at each column top. Transverse strains were monitored both in the steel and in the CFRCM composite through the application of electric strain gages (eSGs). Particularly, four were applied onto the central stirrup at the column mid-height before casting operations, to evaluate TSR strains ($e_{s,xx}$). Four were also used to evaluate

fiber strains ($e_{f,xx}$), applying directly the strain gages onto the carbon sheet, being two per each layer and located in the same position in opposite faces. Their disposition, depending on the specimen type, is shown in Fig. 2. It is worth to recall that all the measures were recorded with same acquisition unit, at same frequency fixed at 5 Hz.

For the damaged specimens, before the application of the FRCM jacket, a repair protocol was followed. First, an inspection of damaged regions of the tested unconfined specimens was carried out, removing the loose concrete with a hammer, and cleaning the surface with an air compressor. The appearance of the specimens at this stage is shown in Fig. 3a. Then, the section of the columns was restored to the original size, using the mortar type described
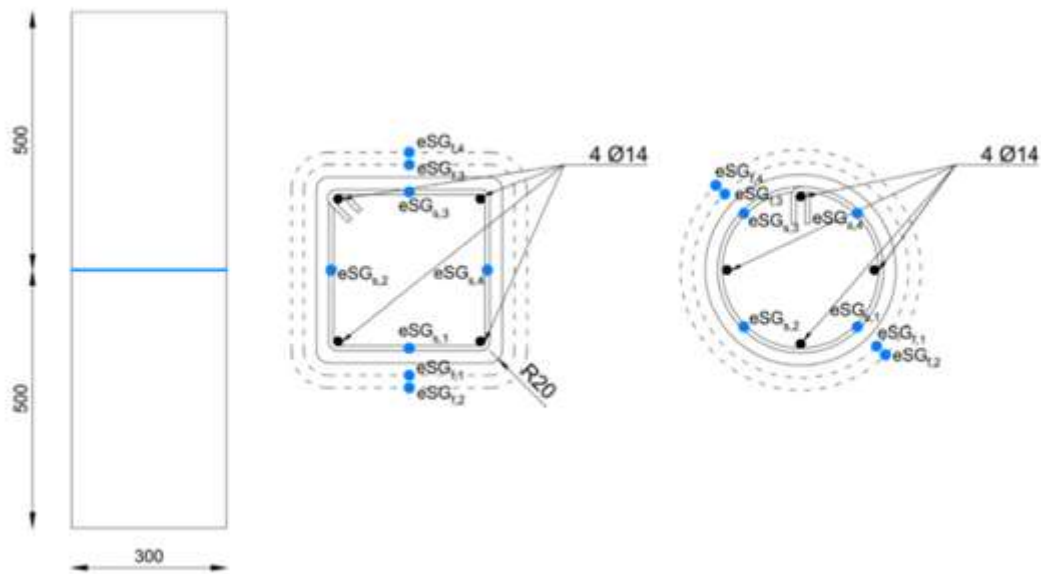
Fig. 2. Disposition of eSGs to evaluate stirrup and fibers strains.

Fig. 3. S33_NC specimen after failure (a); S33_NC specimen after repair operation (b).

in Section 2.2, applying it in layer of maximum 30 mm per time as recommended by the producer, and whose characteristics are listed in Table 2. Before placing the mortar into the formwork, the concrete of the original specimens was wetted to enhance the bond between the two materials. Lastly, after repair operation (see Fig. 3b), concrete surface was superficially damped and covered with plastic wrap for one week.

Concerning instead CFRCM jacketing operation, this was carried out after 28 days from specimens manufacturing in case of strengthened ones, and after 28 days from the repair operation in case of severely-damaged samples. In both cases, the application of the composites followed the

same procedure: first, specimens' surface was wetted to homogenously hydrate the support; then, a first layer of mortar was applied (Fig. 4a), with an average thickness of 3 mm; the first layer of carbon sheet (instrumented with the eSGs) was then allowed to adhere to the mortar, gentle pushing into the matrix; then, the same procedure was repeated, ensuring the sheet to have an overlapping length of about 200 mm. The choice of the overlapping length used was based on a literature review on bond between FRCM systems and concrete substrates. Ombres and D'Ambrisi investigated bond behavior in PBO FRCM – Concrete systems

reporting an effective bond length ranging between 150 mm and 200 mm; Caggegi et al. reported an effective bond length related to Basalt TRM strengthening system of approximately 125 mm; Raof et al. found that the effective bond length is in the range of 200–300 mm depending on the examined number of layers used. The overall thickness of the two CFRCM layers jacket was about 8 mm. It is worth to recall that the sheet was cut having an overall height of about 980 mm, thus leaving about 10 mm of empty surface per side, at the top and bottom of the specimen (Fig. 4b).
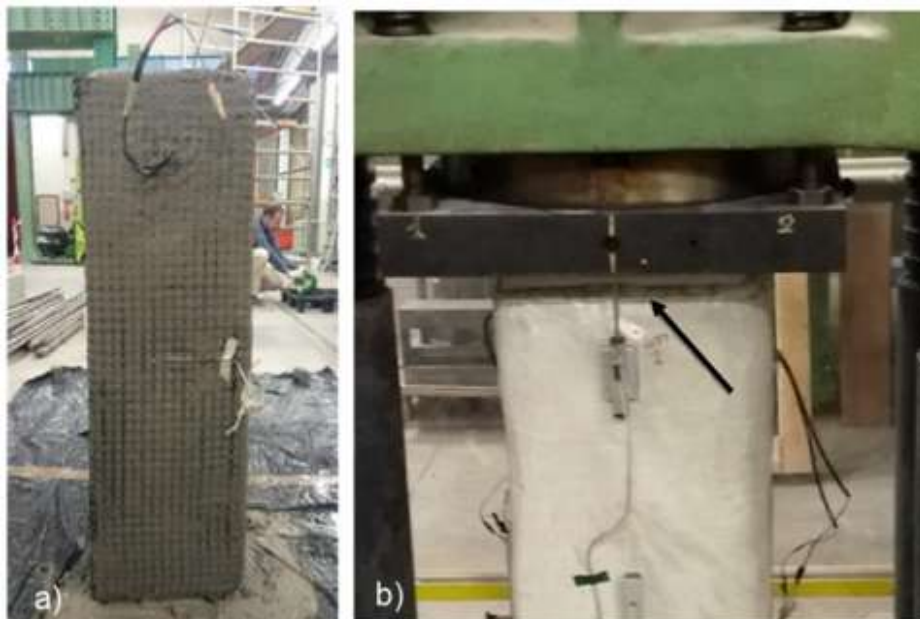

Fig. 4. Application of the first FRCM layer onto the S33_D1_C2 specimen (a); detail of the top of S33_D1_C2 specimen prior to the test (b).

III.   RESULTS

3.1.   Cracking pattern

All nine specimens were tested under monotonical axial compressive load while carefully monitoring axial stresses and strains, crack propagations, and strains development in the inner transverse steel reinforcement and in the outer fiber reinforcement. Collapse achievement, for the sake of comparison, is herein conventionally defined as a 20% reduction of the maximum attained load, both for confined and unconfined specimens, even though loading has been stopped at about 30% of the maximum load drop in the unconfined specimens. Cracks opening and propagation were monitored during the loading history.

For the unconfined specimens, relevant visible cracking patterns occurred mainly in the post-peak branch, while for the confined specimens

cracking displayed much earlier. For these latter, all cylinder specimens displayed a quite uniform cracking pattern in the pre-peak loading while in the post-peak loading very few new openings were observed (Fig. 5). Instead, for the squared columns, existing cracks at the overlapping zone and near the edges grew at a higher rate in the post-peak branch than in the prepeak one. Severely-damaged specimens displayed similar cracking patterns to the undamaged jacketed ones, even though more homogeneous vertical cracks were observed in the damaged squared columns compared to the undamaged ones. It is worth highlighting that confined specimens with higher TSR spacing displayed a wider cracking pattern in both damaged and undamaged conditions.

3.2.   Axial stress–strain behavior
3.2.1. Undamaged bare vs. strengthened specimens

The analyzed columns were cast in two different moments resulting in two different concrete batches, having different compressive strengths but also elastic moduli as highlighted in Section 2. For both batches, important enhancements of the properties were observed even though some differences in the overall axial behavior, that will be shown hereafter, may be due to such initial concrete difference.

Axial behavior is discussed principally in terms of peak axial strength (f_{c0}) and corresponding axial strain (e_{c0}), ultimate concrete stress (f_{cu}) (at 0.8 P_{max}) and corresponding ultimate axial strain (e_{cu}) for the results of the unconfined specimens. For the confined specimens, results are presented in terms of confined axial strength (f_{cc}) and corresponding axial strain (e_{cc}), confined ultimate stress (f_{ccu}) and corresponding ultimate axial strain (e_{ccu}). Concrete axial stresses are computed deducing from the load recorded by the load cell the amount beared by the longitudinal bars, and then dividing it by the section area of the concrete. Recall that failure condition is conventionally considered at 0.8P_{max} but since the load beared by the longitudinal bars is deduced when computing concrete axial stresses, f_{cu} (or f_{ccu}) does not correspond to 0.8 f_{c0} (or f_{cc}). Axial stress–strain curves are shown in Fig. 6 comparing each trio of unconfined (continuous line), strengthened (dashed), and severely-damaged repaired (dotted) specimens.

Clear enhancements of peak strength and peak strain are observed for C20 and S33 confined specimens compared to the unconfined counterparts. Instead, an inconsistent behavior was observed for the S20_D0_C2 specimen: improvements were observed only in terms of ultimate strain, while axial strength remained almost invariant with respect to the unconfined S20_NC counterpart. Even though the same concrete batch was used for both these specimens, differences in concrete compaction and curing is believed to be the cause of this lack of improvement. Also quite low fiber strains were recorded at concrete peak strain for this specimen compared to the S33_D0_C2 and C20_D0_C2 ones. The main parameters resulting from the tests are listed in Table 3.

For undamaged specimens the best results, as expected, are obtained for the circular cross-section column with 34% increase in peak axial strength (f_{cc}) and 28% in peak strain (e_{cc}). The squared section column S33, which also had a higher TSR spacing, showed a 27% improvement in axial strength and only 10% in peak strain. For the S20 specimen, for the reasons mentioned above, strength enhancement was limited but an important increase of 22% was observed in peak strain and nearly 30% in ultimate strain. On the other hand, S33_D0_C2 column was the only to record a slightly lower ultimate strain (92.5%) with respect to the unconfined specimen.

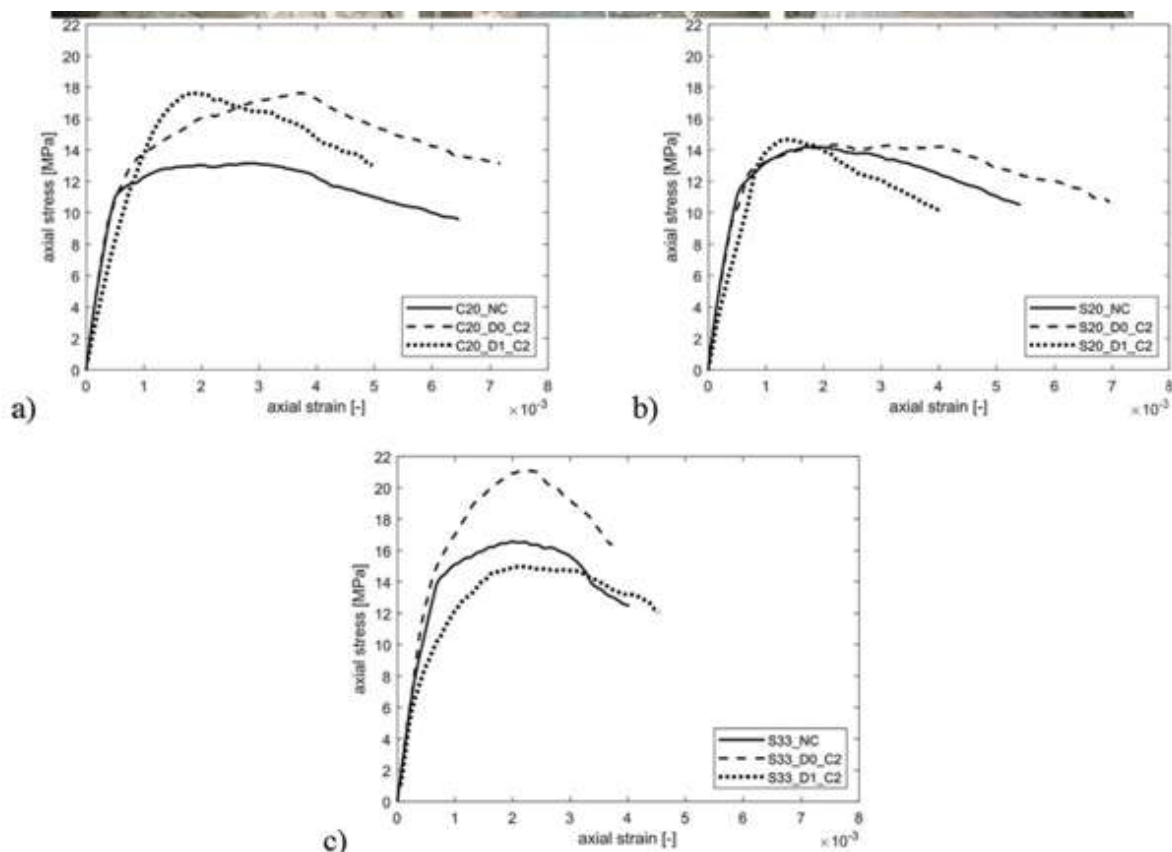Fig. 5. C20_NC, C20_D0_C2 and C20_D1_C2 at the end of the loading history.

Fig. 6. Axial stress strain behavior of the considered unconfined (NC), undamaged strengthened (D0) and damaged repaired (D1) specimens.

Table 3

Specimens test results.

Specimen ID	$f_{c0(cc)}$ [MPa]	$f_{cu(ccu)}$ [MPa]	$f_{u,D}$ [MPa]	$e_{c0(cc)}$ [-]	ecu(ccu) [-]	fcc/fc0 [-]	fccu/fcu [-]	ecc/ec0 [-]	eccu/ecu [-]	fcc/fu,D [-]
C20_NC	13.15	9.62	8.08	0.0029	0.0065	–	–	–	–	–
S20_NC	14.20	10.58	8.38	0.0018	0.0054	–	–	–	–	–
S33_NC	16.58	12.52	10.68	0.0020	0.0040	–	–	–	–	–
C20_D0_C2	17.63	13.21	–	0.0037	0.0072	1.34	1.376	1.276	1.107	–
S20_D0_C2	14.34	10.71	–	0.0022	0.0070	1.01	1.012	1.222	1.296	–
S33_D0_C2	21.09	16.43	–	0.0022	0.0037	1.27	1.312	1.100	0.925	–
C20_D1_C2	17.62	13.02	–	0.0019	0.0050	1.34	1.353	0.655	0.770	2.180
S20_D1_C2	14.67	10.20	–	0.0014	0.0040	1.03	0.964	0.777	0.741	1.750
S33_D1_C2	14.98	12.05	–	0.0022	0.0046	0.90	0.962	1.100	1.150	1.402

3.2.2. Severely-damaged repaired specimens

The main focus of the presented work is to assess the effectiveness of CFRCM confinement on repairing severely damaged RC columns, and quite promising results were observed for the three specimen types considered, as shown in Fig. 6. A clear improvement in terms of axial strength with respect to the damaged conditions is observed for all specimens. As for the undamaged columns, the best performance was observed for the C20 geometry which was able to equal the attained load of the undamaged strengthened specimen, showing an increase of nearly 34% in axial strength with respect to the unconfined case. In the square section columns, as expected, CFRCM confinement resulted less effective than their analogue circular one. The repair was able to restore the initial strength of S20_NC (with also 3% gain) in the S20_D1_C2 specimen; instead, in the S33_D1_C2 the repair procedure was able to restore only 90% of the initial unconfined strength of S33_NC (see Table 3).

Looking at the overall stress–strain curves of undamaged specimens, in the pre-peak branch no significant differences in the axial stiffness are noted between unconfined and confined columns. As can be seen in Fig. 6, differences are observed only after stress values near to f_{c0} value. On the other hand, damaged specimens show immediately a reduced axial stiffness due to their damaged condition. But while specimens with the same TSR spacing (s = 200 mm) show similar elastic modulus reduction regardless of the cross section shape, specimen S33_D1_C2 displays a more pronounced difference between undamaged and damaged secant modulus since relatively small stress values (nearly to 6 MPa). As damage level is relatively similar in all specimens, it is believed that TSR high spacing is the main factor to which this difference is due.

When considering undamaged RC columns confined with CFRCM, the confinement system effectiveness seems similar in terms of peak strength (f_{cc}) and strain (e_{cc}) development, with gains varying in the order of 10–34%, as discussed in Section 3.2.1. This is not the case when dealing with severely damaged columns. The CFRCM system for the damaged columns with the lowest TSR spacing (i.e., C20 and S20) was able to restore at least the initial strength of the unconfined specimens. However, in none of the above, it was possible to restore the peak strain of the unconfined specimens, reaching only 65% and 78% of e_{c0}, respectively. The confined damaged specimen with the highest TSR spacing (i.e., S33_D1_C2) could not restore the initial unconfined strength, probably due to its lower axial stiffness previously discussed,

and reached its peak strength at an axial strain 10% higher than its unconfined case.

However, when assessing the effectiveness of CFRCM confinement on repairing severely-damaged RC elements, the authors believe that it is not entirely appropriate to refer to the initial resistance of the undamaged condition only. Indeed, since repairing is done on an already damaged element, it results more significant to evaluate the effectiveness of the intervention referring to the residual axial strength of the columns at the end of the previous loading history. In Table 3, the residual axial strength values for each unconfined specimens are reported under the parameter $f_{u,}$ D, and the effectiveness of the repair operation is evaluated through the $f_{cc}/f_{u,D}$ ratio. It can be seen that through the CFRCM confinement, all repaired specimens have significantly enhanced their residual axial capacity. The circular-shaped section is still the most effective with an increment of the repaired axial capacity with respect to the residual capacity of the severely-damaged element of nearly 118%. The squared-shape sections result less effective than the circular one, but were still able to enhance their damaged residual capacity by 73% for the S20_D1_C2 and by 41% for the S33_D1_C2 specimen. It is important to highlight how, apart from the influence of the cross-section shape in the effectiveness of the CFRCM confinement, the spacing of internal TSR is of fundamental importance in the overall confinement effectiveness.

3.3. Fiber and TSR strain development

Strain development was monitored in all specimens in the central stirrup using four eSGs and in the FRCM layers for the externally confined specimens using two eSGs per layer applied on the opposite faces of the columns, as better detailed in Section 2.3. Results are shown in Figs. 7 and 8 for unconfined (continuous line), strengthened (dashed), and severely-damaged repaired (dotted) specimens. Fully opaque lines represent the mean strain values while transparent lines show the trend of single eSGs.

3.3.1. TSR strains

Fig. 7 shows in detail TSR strains evolution in (a) C20, (b) S20 and (c) S33 columns, in all the three analyzed conditions. The circular-section C20 geometry recorded the lowest strains compared to the square-section columns for all three considered conditions. Particularly low strain values were recorded in the unconfined and strengthened specimens (i.e., C20_NC and C20_D0_C2). This may be due to damage

concentration on the upper part of the column which may have solicited more those stirrups in the highest positions (see Fig. 5), which unfortunately were not being monitored.

For the undamaged columns, strains in the TSR grow at the same rate in both confined and unconfined elements. A slight difference is noted only in the S33 undamaged specimens, where at axial stress of about 9 MPa the TSR strain rate becomes slightly higher for the unconfined specimen. Generally, TSR strains development started earlier for damaged specimens, which also developed higher values than the undamaged ones. It is interesting to notice the difference in the strain rate development between circular- and square-section columns. Strain rates in the pre-peak branch of the curve result much higher for the squared shape sections, while the circular one shows strain rates closer to the undamaged conditions, which grow faster at axial stress levels near to the unconfined strength (f_{c0}). For damaged square-section columns (i.e., S20_D1_C2 and S33_D1_C2) TSR strains grow at higher rates after stress levels of about 0.25–0.30 f_{cc}.

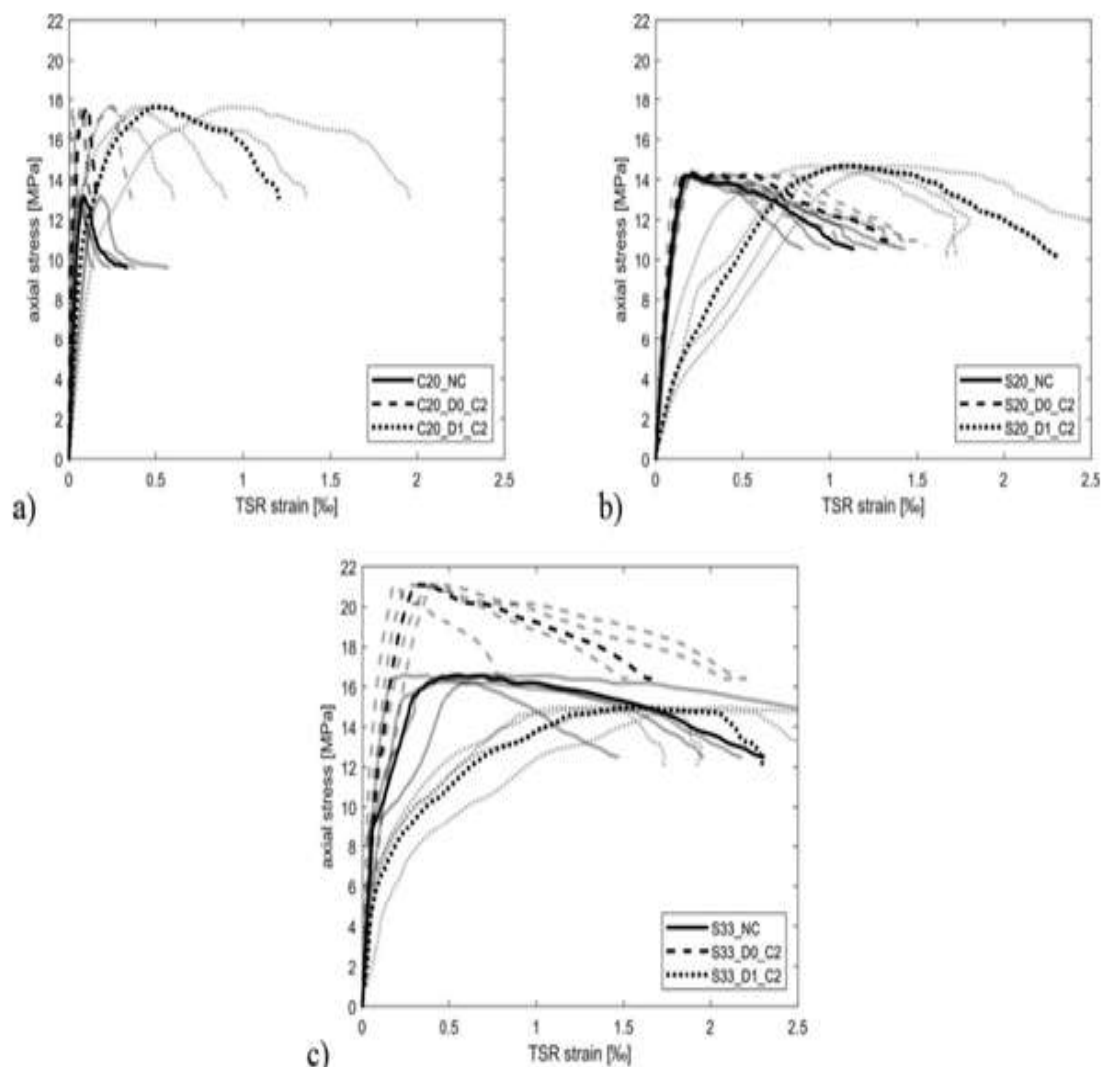
Fig. 7. Axial stress – TSR strains for unconfined, undamaged strengthened and damaged repaired columns. (a) C20, b) S20 and c) S_33 specimens.
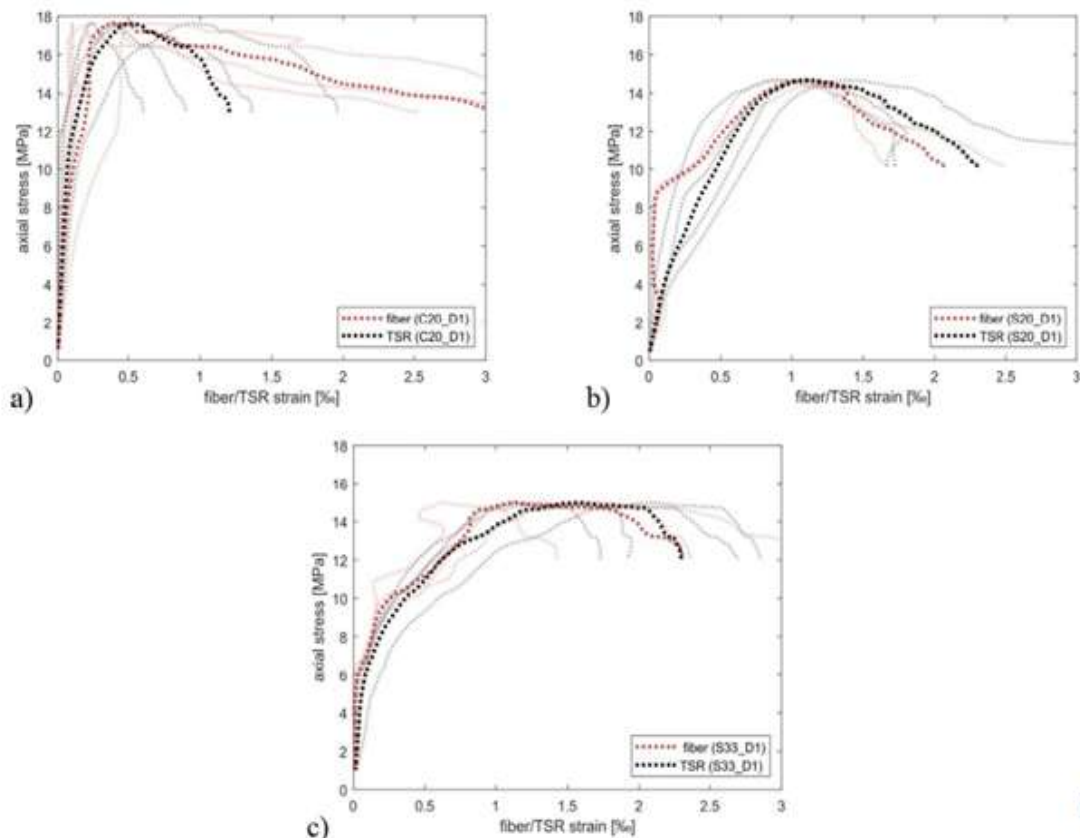
Fig. 8. Axial stress – fiber and TSR strain for damaged repaired specimens. a) C20_D1_C2, b) S20_D1_C2, c) S33_D1_C2.

Table 4 reports mean strain values for TSR and FRCM at peak and ultimate stresses. Comparing TSR strains at peak load among undamaged specimens, very similar values are recorded. $e_{s,xx}$ of the C20_NC is a little less than 0.1‰, while also the confined one C20_D0_C2 recorded strains slightly above 0.1‰. The squared S20 undamaged specimens recorded also similar TSR strains of nearly 0.18‰ and 0.20‰, respectively for the unconfined and confined situations. On the other hand, the S33 specimens recorded lower TSR strains in the confined condition (0.33‰) with respect to the unconfined one (0.68‰). It seems that higher TSR strain values at peak stress are recorded in specimens with less effective confinement systems, both in terms of section-shape and reinforcement spacing. This order is maintained also for TSR strains at ultimate stress with higher strains recorded in the S33 column followed by the S20 and C20 ones.

Discussing the strain evolutions on damaged columns (i.e., those specimens labelled with ''D1''), the results show TSR strains at peak load that are almost five times higher than the ones recorded in the confined but undamaged cases (i.e., D0).

Table 4
Mean TSR and fiber hoop strains at peak and ultimate stress.

Specimen ID	es,xx (peak) [‰]	es,xx (ultimate) [‰]	ef,xx (peak) [‰]	ef,xx (ultimate) [‰]
C20_NC	0.0877	0.3585	–	–
S20_NC	0.1762	1.1826	–	–
S33_NC	0.6764	2.3388	–	–
C20_D0_C2	0.1073	0.1646	0.2172	0.2805
S20_D0_C2	0.1971	1.3880	0.1264	0.4285
S33_D0_C2	0.3258	1.7170	0.2520	0.6281
C20_D1_C2	0.5070	1.2074	0.4017	3.2342
S20_D1_C2	1.1069	2.3229	1.0629	2.0963
S33_D1_C2	1.5811	2.3113	1.1363	2.3398

C20_D1_C2 specimen recorded a mean TSR strain of 0.5‰ (instead of 0.1‰ recorded in C20_D0_C2), S20_D1_C2 TSR strain was about 1.1‰ (instead of 0.2‰ in S20_D0_C2) and the same trend was observed in the S33 geometry, where the damaged case S33_D1_C2 recorded 1.58‰ (instead of 0.33‰ in S33_D0_C2).

3.3.2. Fiber and TSR strains in the confined columns

Measuring local strains in the FRCM jacketing experimentally is a harsh task and not always repays with the expected results. The possibility that cracks open at eSG location or that eSGs are located between two cracks, being so affected by tension stiffening phenomena, may result in quite variable strain records. To guarantee reliable results, high numbers of eSGs distributed through the reinforcement layers must be applied, but this cost efforts and especially can result uneconomic. However, in this experimental campaign good results were obtained also for the monitored fiber strains. Few eSGs with discordant records were discarded from the final results.

Fig. 8 compares TSR and fiber strains in the damaged specimens in (a) C20_D1_C2, (b) S20_D1_C2 and (c) S33_D1_C2 specimens, while fiber strain values at peak and ultimate stress are listed in Table 5, in its last two columns. In the pre-peak condition, C20_D1_C2 and S33_D1_C2 develop TSR and fiber strains at almost the same rate. In the S20_D1_C2 specimen, significant fiber strains were recorded only after stress levels of nearly 0.6 f_{cc}, while TSR strains start growing almost immediately. Different trends are observed in the post-peak branch for circular- and square-section specimens. In the C20_D1_C2 specimen, after peak stress, fiber strains grow at higher rate than TSR strains. This means that the FRCM system plays a bigger role than the TSR in the axial ductility of the confined RC element. In both square-section columns, TSR and fiber strains follow almost the same trend in the post-peak behavior, with TSR final strains being slightly higher than the fiber ones in the S20 case and almost the same strains in the S33 geometries. Peak strains recorded in TSR and fibers were quite similar in all specimens, with some differences only in the S33 specimen. The circular-section column C20_D1_C2 recorded lower peak strain values (0.4‰ for fibers and 0.5‰ for TSR) compared to those in squared columns, which were more than the double. On the other hand, fiber strains at ultimate stress were higher in the circular shaped section, which explains, along with the more effective section shape, the slightly more ductile behavior this specimen showed (Fig. 6).

It is also worth mentioning that in C20 and S20 specimens no significant differences were noted in the strains recorded in the different layers of the CFRCM system while in the S33 specimens fiber exploitation resulted higher in the first CFRCM layer.

IV. DISCUSSION

4.1. Cross-section geometry effect

Cross-section shape is known to be an important factor when dealing with confinement systems and its influence remains important even when repairing damaged RC elements. Fig. 9 compares axial stress–strain curves relative to the initial strength of unconfined specimens f_{c0} (a) and to the remaining capacity of the damaged specimens $f_{u,D}$ (b). Cross-section shape effect is evident when comparing C20 and S20 geometries, characterized by the same TSR and fiber rate. C20_D1_C2 specimen results nearly 30 % more effective than the squared-shape column in terms of both $f_{cc}/f_{u,D}$ and f_{cc}/f_{c0} rates. On the other hand, TSR influence on the overall behavior of the repaired elements is well highlighted comparing specimens S20 and S33, that differ only by the stirrups

spacing (i.e. 200 and 330 mm). The effect of stirrup spacing is clearer in Fig. 9.b, which considers the repaired strength f_{cc} with respect to the residual strength $f_{u,D}$ of the damaged specimens. The repaired S20 specimen resulted 25% more effective than the same specimen with 330 mm stirrup spacing (S33). Comparing f_{cc}/f_{c0} rates only, the S20 specimens would result only 14% more effective than the S33. These results indicate that cross-section shape and fiber-TSR interaction can significantly influence the overall behavior of damaged elements repaired through CFRCM confinement.

Cross-sectional shape influences also the development of lateral strains in TSR and fiber

reinforcement. Fig. 10 compares lateral TSR strains in unconfined (a) and in strengthened specimens (b). Similar trends can be seen between NC and D0_C2 series: there, square- shaped columns record higher lateral stirrup strains in both confined and unconfined cases. Also, in the post-peak branch, TSR strains tend to decrease faster in the circular shape with respect to the squared ones. Fig. 11 shows TSR strains (a) and fiber strains (b) for the damaged specimens, showing the same trend described before about the influence of cross-section geometry on the development of e_{xx} in the central stirrup.

| Specimen ID	q_s	k_s	q_f	k_f	fls [MPa]	flf [MPa]	fl,tot [MPa]	fls [MPa]	flf [MPa]	fl,tot [MPa]
C20_NC	0.00387	0.403	–	–	0.014	–	0.014	0.059	–	0.059
S20_NC	0.00387	0.197	–	–	0.014	–	0.014	0.095	–	0.095
S33_NC	0.00234	0.067	–	–	0.009	–	0.009	0.038	–	0.038
C20_D0_C2	0.00387	0.403	0.00125	1.000	0.018	0.033	0.050	0.027	0.043	0.069
S20_D0_C2	0.00387	0.197	0.00125	0.499	0.016	0.010	0.025	0.111	0.032	0.144
S33_D0_C2	0.00234	0.067	0.00125	0.499	0.005	0.019	0.024	0.028	0.048	0.076
C20_D1_C2	0.00387	0.403	0.00125	1.000	0.083	0.061	0.144	0.197	0.490	0.688
S20_D1_C2	0.00387	0.197	0.00125	0.499	0.089	0.080	0.169	0.186	0.159	0.345
S33_D1_C2	0.00234	0.067	0.00125	0.499	0.026	0.086	0.112	0.038	0.177	0.215
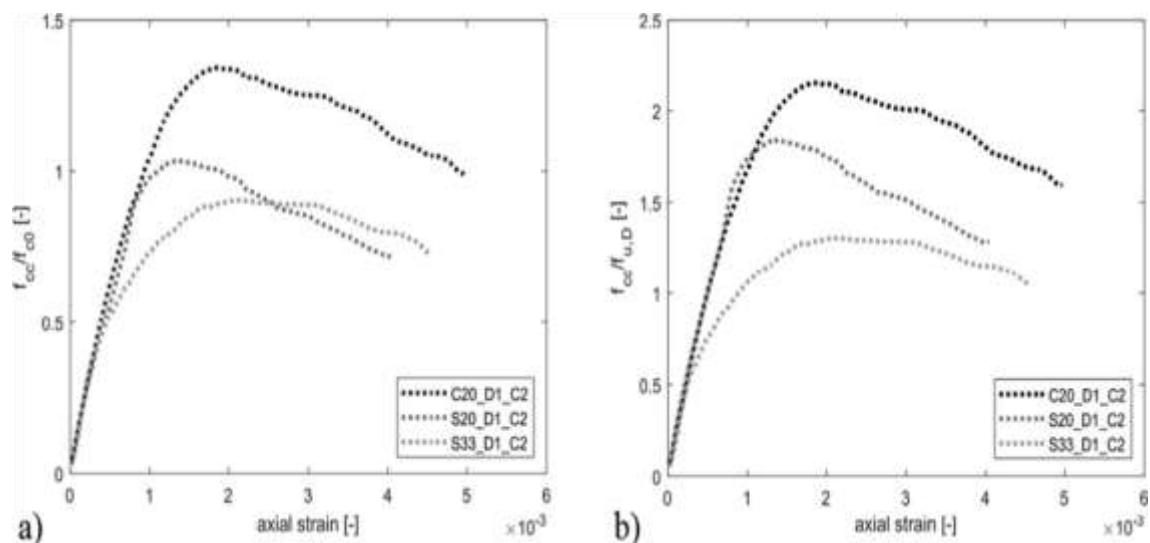
Fig. 9. Relative axial stress – strain curve with respect to the undamaged cases (a) and to the residual axial capacity of the damaged specimens (b).
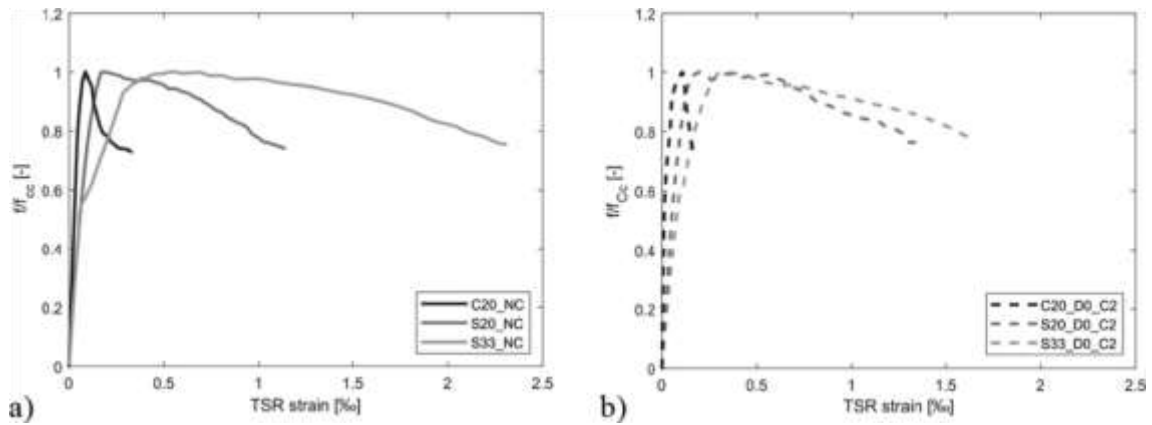
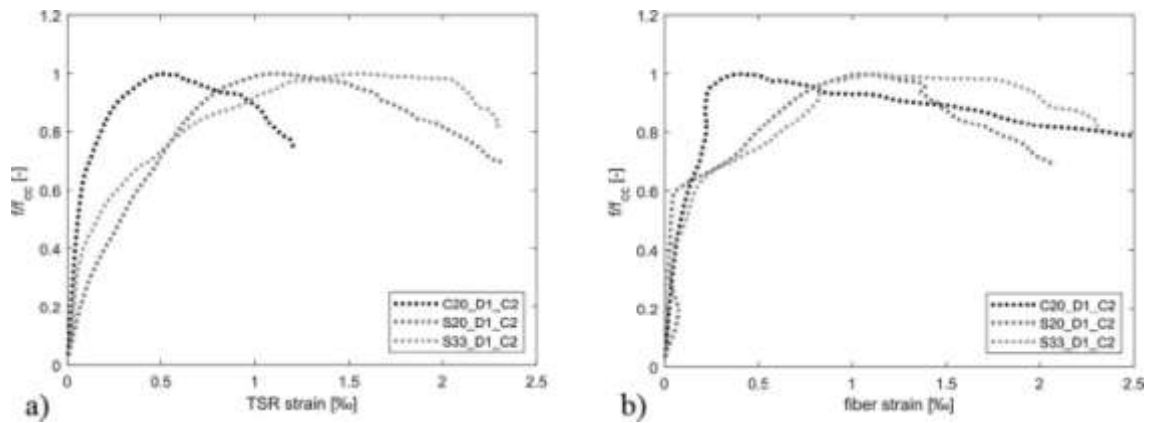Fig. 10. TSR strains in unconfined (a) and in undamaged strengthened specimens (b).

Fig. 11. TSR (a) and fiber (b) strains in the damaged repaired specimens.

4.2. Lateral pressure and Fiber-TSR interaction

Generally, confinement effectiveness is considered in concrete confinement models whether they are dealing with internally confined (TSR) or externally (FRP, FRCM) confined concrete, through effectiveness coefficients (k_s & k_f). For continuous FRCM jacketing the horizontal efficiency coefficient $k_{f,h}$ depends on the corner radius r and on the cross-section dimensions b and h for rectangular shape, while for circular cross-section this coefficient is assumed to be unitary.'

Other effectiveness coefficients can be considered to account for fiber orientation with respect to the member axial axis ($k_{f,a}$) or for vertical efficiency in partially wrapped systems ($k_{f,v}$), which are assumed unitary for the analyzed configurations used in this experimental campaign.

For internal confinement by TSR, the geometric effectiveness coefficient does not depend on corner radius but only on the layout and spacing of TSR and can be computed following the Mander et al. approach [48] for circular cross-sections:

$$\frac{\left(b-2r\right)^2 + \left(h-2r\right)^2}{3bh} + k_{f,h} = 1 \qquad 1$$

Other effectiveness coefficients can be considered to account for fiber orientation with

$$\frac{k_s \frac{1}{4} \delta A_e \rth \frac{1}{4} \delta 1 s 0 = 2 d s \rth \delta 2 \rth}{1 q_{cc} A_c \quad 1 q_{cc}}$$

and for rectangular ones:

$$\frac{\delta^1 P n i \frac{1}{4} 1 \delta 6 w b c 0 i d \rth c 2 \rth \delta^1 2 \underline{s} b 0 c \rth \delta 1 2 \underline{s} d_c \rth \delta \rth k_s \frac{1}{4} \delta \quad \rth 3}{1 q_{cc}}$$

where A_e is the effectively confined concrete area; A_c is the concrete core area; q_{cc} is the longitudinal reinforcement ratio to the core area; s^0 is the clear vertical spacing between consecutive stirrups; d_s is the hoop diameter for circular cross-sections; w^0_i is the i- th clear distance between adjacent longitudinal bars; b_c and d_c are the concrete core dimensions taken between stirrups centerlines. Once the effectiveness coefficients are known, the lateral confining pressure can be computed for both internal TSR:

$$f_{ls} \frac{1}{4} \frac{1}{2} \_k_s q_{st} r_{st} \quad \delta 4 \rth$$

and external FRCM system:

$$f_{lf} \frac{1}{4} \_\frac{1}{2} k_f q_f r_f \quad \delta 5 \rth$$

where q_{st} and q_f are the volumetric ratio of TSR and FRCM and r_{st} and r_f are stresses in stirrup and fibers.

For rectangular cross-sections, the confining pressure should be computed separately in the two main directions ($f_{ls;x}$ and $f_{ls;y}$) , since for non-symmetrical sections lateral pressure can be different. Mander et al. sets r_{st} equal to the yielding stress of the reinforcement.

Pellegrino & Modena studied the interaction between internal TSR and external FRP confinement proposing an additive model to compute the overall confining pressure offered by both systems. However, such interaction is not yet studied for FRCM confining systems and existing models generally neglect TSR contribution. The issue is even less clear when it comes to repairing and not just strengthening of existing structures. To investigate this phenomenon, strain data on both fibers and TSR were collected experimentally through electrical strain gages. The experimental data gathered in this campaign suggest that, at least

for damaged elements, TSR contribution and fiber-TSR interaction are important factors in the behavior of damaged RC elements repaired through FRCM confinement, since they grow at similar rates both in the pre- and post-peak branches of stress–strain curves.

Fiber and TSR mean strain values for peak and ultimate load are reported in Table 4. Based on these strain values and on the effectiveness coefficients computed as shown in the above equations, confining pressure exerted by TSR and FRCM at peak and ultimate (80%) load was computed and reported in Table 5. Also, the total confining pressure $f_{l,tot}$, computed as the sum of TSR and fiber pressure, is given for peak and ultimate load.

It can be noted that the confining pressure exerted by TSR (f_{ls}) at peak load is almost the same for specimens with the same stirrup spacing regardless of their cross-section. TSR confining pressure is significantly lower for the S33 geometries than in all other cases. On the other hand, FRCM provides continuous confinement to the columns and is more influenced by cross-section shape than TSR, thus varying more between prismatic and cylinder columns. For damaged and repaired columns, confining pressure at peak load exerted by fibers results similar for S20 and S33 specimens, while the circular one (C20) displays slightly smaller lateral pressure. This value becomes much bigger in the post-peak branch, exceeding largely those values recorded by the specimens with the square cross-section.

In the S33 specimens, FRCM contribution to the overall confinement results significantly higher than the TSR effect. Instead, for 200 mm stirrup spacing, fiber and TSR contribution to the overall confining pressure at peak load becomes similar, even though, a higher TSR effect is seen in the circular section. At the ultimate load, FRCM confining pressure results more than double the TSR pressure in the circular shaped specimens while in the squared one the two pressures result quite comparable. Considering the total confining pressure as a simple addition of the TSR and fiber contributions, the highest value (0.169 MPa) at peak load is recorded in the S20 specimens while for ultimate load in the C20 one (0.688 MPa). In the undamaged specimens, fiber confining pressure resulted in smaller and more dispersive values.

The results in terms of lateral confinement pressure highlight how neglecting the contribution of transverse reinforcement, as existing models on FRCM confinement of concrete currently do, is an assumption that does not reflect the actual behavior, at least for elements with not too large stirrups

spacing. In addition, recalling the results in terms of strength enhancement after repair, where the circular-shaped column performed undoubtedly better than the squared-section ones, results show also that a simple additive contribution of the two reinforcements does not well describe the overall behavior and particularly the interaction of the two reinforcements under the axial loading.

V. CONCLUSIONS

The analytical work presented in this paper aimed to study the effectiveness of FRCM systems to adequately repair RC columns through confinement. Two different cross-section shapes (circular and squared) and two TSR spacing (200 and 330 mm) were considered in full-scale specimens. Results of repaired specimens were then compared to the results of unconfined undamaged specimens and FRCM confined undamaged RC specimens. Hoop strains were monitored in both TSR and fibers to evaluate the effective confining pressure and possible interaction between internal and external confining systems. Based on the experimental results previously discussed, the following conclusions can be drawn: repair through CFRCM confinement was able to enhance concrete strength in all considered specimens. Compared to the residual axial capacity of the damaged specimens, the repair protocol was able to enhance concrete strength by a factor of 2.18 in the circular-shaped C20_D1 specimen, 1.75 in the squared-shape S20_D1 and 1.40 in the squared-shape S33_D1

Specimen;cross-section shape and TSR spacing have an important effect in the overall repair effectiveness. The circular-shaped specimen C20_D1_C2 was able to match the resistance of the undamaged FRCM confined C20_D0_C2 specimen while the squared S20_D1_C2 equaled the undamaged C20_NC resistance. The squared specimen with higher TSR spacing was able to reach only 90% of the S33_NC strength; peak and ultimate axial strain did not improve much in all repaired specimens and resulted in lower values with respect to the NC series, apart specimen S33_D1_C2 which stress–strain curve resulted in a slightly different trend with respect to the other two;damaged specimens developed lateral strains in TSR and fibers at higher rates than undamaged ones. Higher strain values were recorded in specimens with less effective confining systems due to both section-shape and TSR ratio. Similar trends were noted for TSR and fiber strains in all specimens; estimated confining pressure exerted by TSR and FRCM confinement highlights the importance of TSR spacing and the results seems to suggest that a simple additive model of the two contributions (fiber & TSR) might not be the best solution to describe the interaction between the internal and external confining systems.

It is important to emphasize that further research on this issue is needed given the lack of existing studies that experimentally investigate FRCM-TSR interaction in concrete confinement and the limited number of specimens, due to their real scale dimensions, investigated in the present one.

Declaration of Competing Interest
The authors declare that they have no known competing financial interests or personal relationships that could have appeared to influence the work reported in this paper.

REFERENCES

[1]. F.J. McGarry, Building design with fibre reinforced materials, Proc. R. Soc. London. A. Mathem. Phys. Sci. 319 (1536) (1970) 59–68.

[2]. M.N. Fardis, H.H. Khalili, FRP-encased concrete as a structural material, Mag. Concr. Res. 34 (121) (1982) 191–202.

[3]. G. Campione, P. Colajanni, L. La Mendola, N. Spinella, Ductility of reinforced concrete members externally wrapped with fiber-reinforced polymer sheets, J. Compos. Constr. 11 (3) (2007) 279–290.

[4]. A. Mirmiran, M. Shahawy, M. Samaan, H.E. Echary, J.C. Mastrapa, O. Pico, Effect of column parameters on FRP-confined concrete, J. Compos. Constr. 2 (4) (1998) 175–185.

[5]. C. Pellegrino, C. Modena, Analytical model for FRP confinement of concrete columns with and without internal steel reinforcement, J. Compos. Constr. 14 (6) (2010) 693–705.

[6]. R. Realfonzo, A. Napoli, Concrete confined by FRP systems: confinement efficiency and design strength models, Compos. B Eng. 42 (4) (2011) 736–755.

[7].   H. Saadatmanesh, M.R. Ehsani, L. Jin, Repair of earthquake-damaged RC columns with FRP wraps, ACI Struct. J. 94 (1997) 206–215.

[8].   G. Li, S. Hedlund, S.-S. Pang, W. Alaywan, J. Eggers, C. Abadie, Repair of damaged RC columns using fast curing FRP composites, Compos. B Eng. 34 (3) (2003) 261–271.

[9].   F. Faleschini, J. Gonzalez-Libreros, M.A. Zanini, L. Hofer, L. Sneed, C. Pellegrino, Repair of severely-damaged RC exterior beam-column joints with FRP and FRCM composites, Compos. Struct. 207 (2019) 352–363.

[10]. R. Eid, P. Paultre, Analytical model for FRP-confined circular reinforced concrete columns, J. Compos. Constr. 12 (5) (2008) 541–552.

[11]. J.G. Teng, G. Lin, T. Yu, Analysis-oriented stress-strain model for concrete under combined FRP-steel confinement, J. Compos. Constr. 19 (5) (2015) 04014084.

[12]. G. Lin, T. Yu, J.G. Teng, Design-oriented stress–strain model for concrete under combined FRP-steel confinement, J. Compos. Constr. 20 (4) (2016) 04015084.

[13]. A. Al-Rahmani, H. Rasheed, Combined Transverse steel-external FRP confinement model for rectangular reinforced concrete columns, Fibers 4 (1) (2016)8.

[14]. S. Kaeseberg, D. Messerer, K. Holschemacher, Experimental study on concrete under combined FRP–steel confinement, Materials 13 (20) (2020) 4467.

[15]. G.C.Z. Bournas, D.A. Tetta, L.A. Bisby, Concrete confinement with TRM versus FRP jackets at elevated temperatures, Mater. Struct. 53 (2020) 58.

[16]. F. Lionetto, M.A. Aiello, A. Maffezzoli, Reversible FRP-confinement of heritage masonry columns, 9th International Conference on Fibre-Reinforced Polymer (FRP) Composites in Civil Engineering (CICE), 2018.

[17]. J. Zhao, V.M. Vokkarane, Reverse manycast data retrieval in Elastic Optical Networks, in: 2017 International Conference on Computing, Networking and Communications (ICNC), Santa Clara, CA, 2017, pp. 402-407, doi: 10.1109/ ICCNC.2017.7876162.

[18]. F. Bencardino, C. Carloni, A. Condello, F. Focacci, A. Napoli, R. Realfonzo, Flexural behaviour of RC members strengthened with FRCM: State-of-the-art and predictive formulas, Compos. B Eng. 148 (2018) 132–148.

[19]. L.H. Sneed, S. Verre, C. Carloni, L. Ombres, Flexural behavior of RC beams strengthened with steel-FRCM composite, Eng. Struct. 127 (2016) 686–699.

[20]. S.M. Raoof, L.N. Koutas, D.A. Bournas, Textile-reinforced mortar (TRM) versus fibre-reinforced polymers (FRP) in flexural strengthening of RC beams, Constr. Build. Mater. 151 (2017) 279–291.